Electronic Supplementary Information

A new antiferromagnetic Dy_6 oxido–material as a multifunctional aqueous phase sensor for picric acid as well as Fe^{3+} ions

Mukul Raizada[a,b]*, M. Shahid[a]*, Sameer Hussain[c], Mo Ashafaq[a], Zafar A. Siddiqi[a]

[a] Functional Inorganic Materials Lab (FIML), Department of Chemistry, Aligarh Muslim University, Aligarh-202002, India.
[b] Current Address, Molecular Magnetism Lab, Department of Chemistry, IISER, Bhopal, India.
[c] Department of Chemistry, Xi'an Jiaotong University, China, PR.
†Corresponding authors, E-mail: shahid81chem@gmail.com, mukulraizada1@gmail.com

Formula for calculating the percentage of Picric acid fluorescence intensity quenching:

$$(Io-I)/Io \times 100\%$$

Where, Io = initial fluorescence intensity,

I = intensity of **1** containing PA solution.

Stern-Volmer equation:

$$I_0/I = K_{SV}[A] + 1$$

Where, I_0 = fluorescent intensity of **1** before the addition of the analyte

I = fluorescent intensity after the addition of the respective analyte

K_{SV} = Stern-Volmer constant

[A] = molar concentration of the analyte (M^{-1}).

Reference: (a) S. Pramanik, C. Zheng, X. Zhang, T. J. Emge and J. Li, *J. Am. Chem. Soc.*, 2011, **133**,4153; (b) D. Banerjee, Z. Hu and J. Li, *Dalton Trans.*, 2014, **43**, 10668.

Table S1. Bond valence sum calculation of Oxygen (O) oxidation state in the crystal structure of **1**

Oxygen atoms	BVS	Assigned protonation levels
O1W	0.25	H_2O
O2W	0.30	H_2O
O3W	0.30	H_2O
O4W	0.30	H_2O
O5W	0.31	H_2O
O6W	0.28	H_2O
O2	1.20	OH^-
O3	1.16	OH^-
O4	1.18	OH^-
O5	1.19	OH^-
O1	1.57	O^{2-}

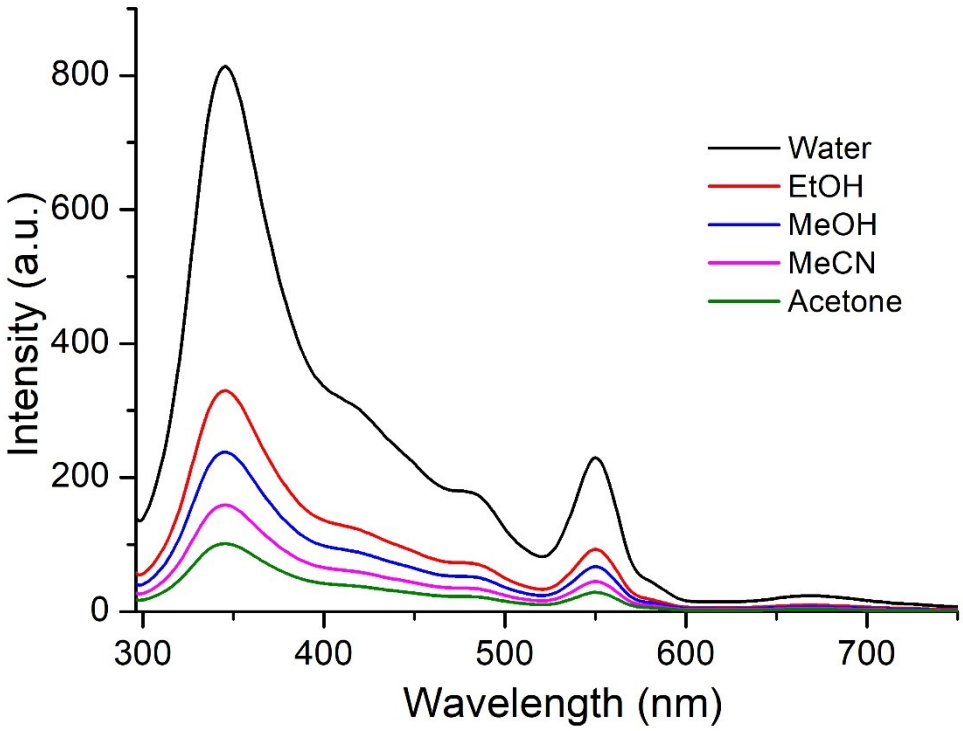

Fig. S1: Emission spectrum of **1** dispersed in different solvents upon excitation at 296 nm.

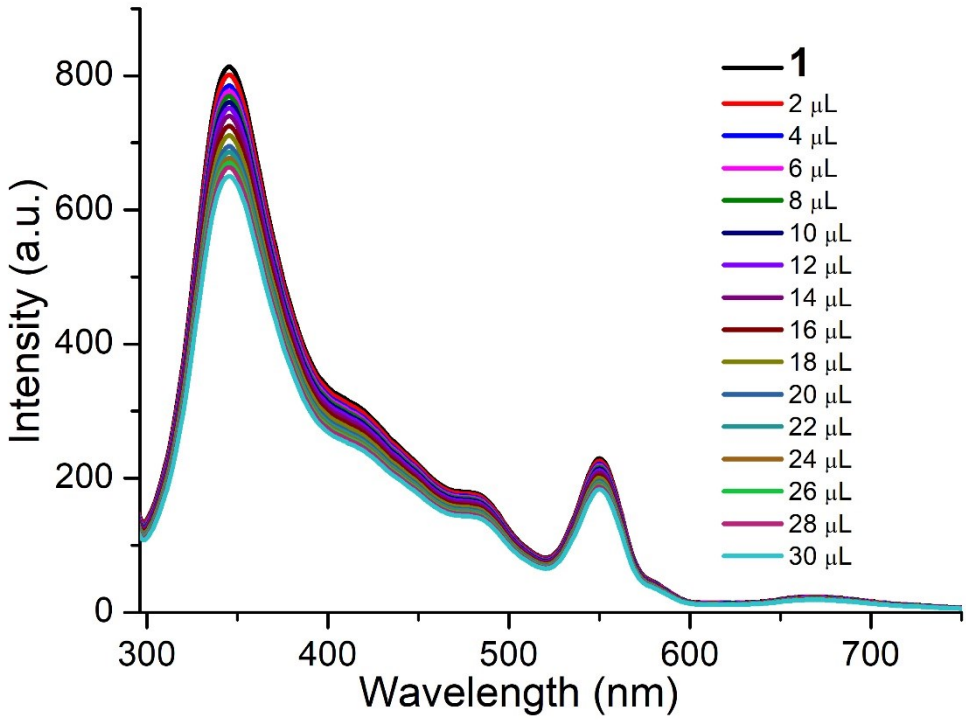

Fig. S2: The change in fluorescence intensity of **1** upon incremental addition of NB solution in Water.

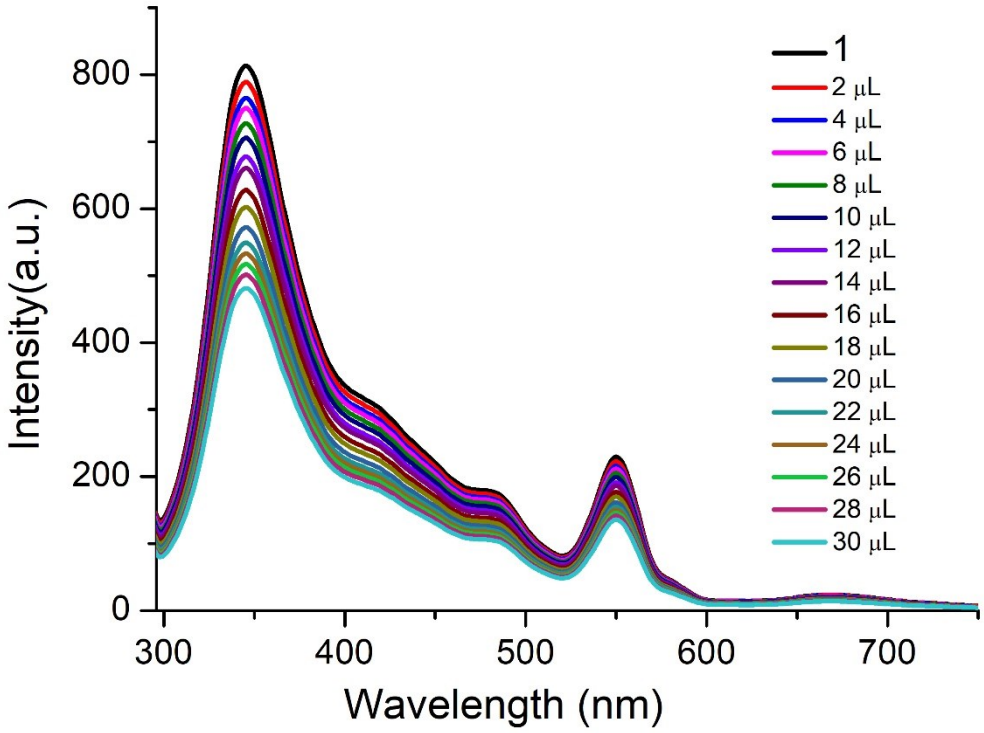

Fig. S3: The change in fluorescence intensity of **1** upon incremental addition of MNP solution in Water.

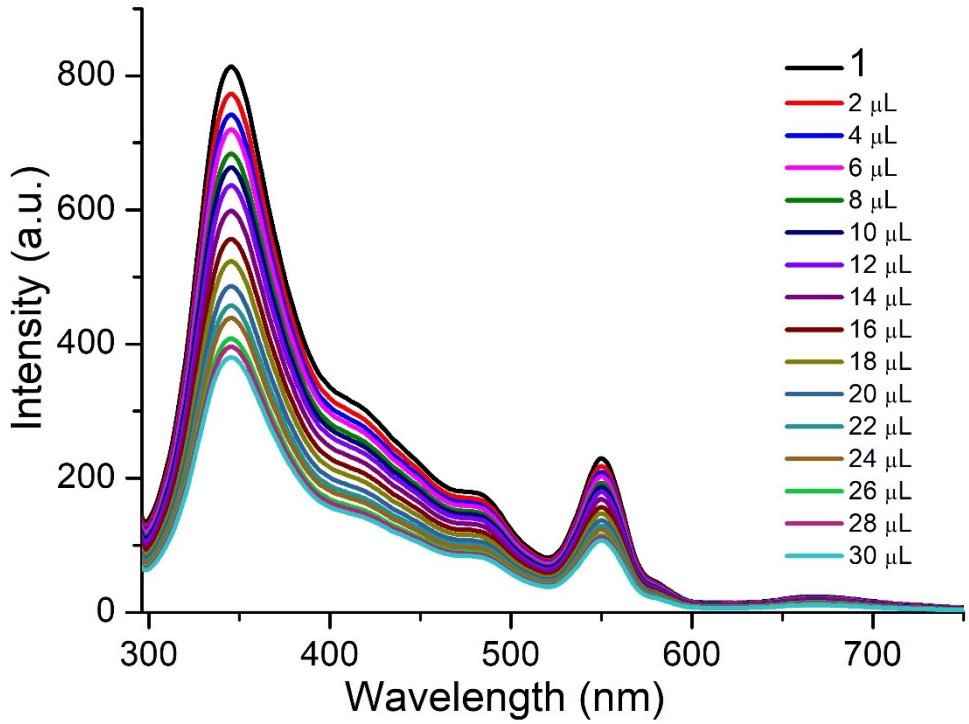

Fig. S4: The change in fluorescence intensity of **1** upon incremental addition of PNP solution in Water.

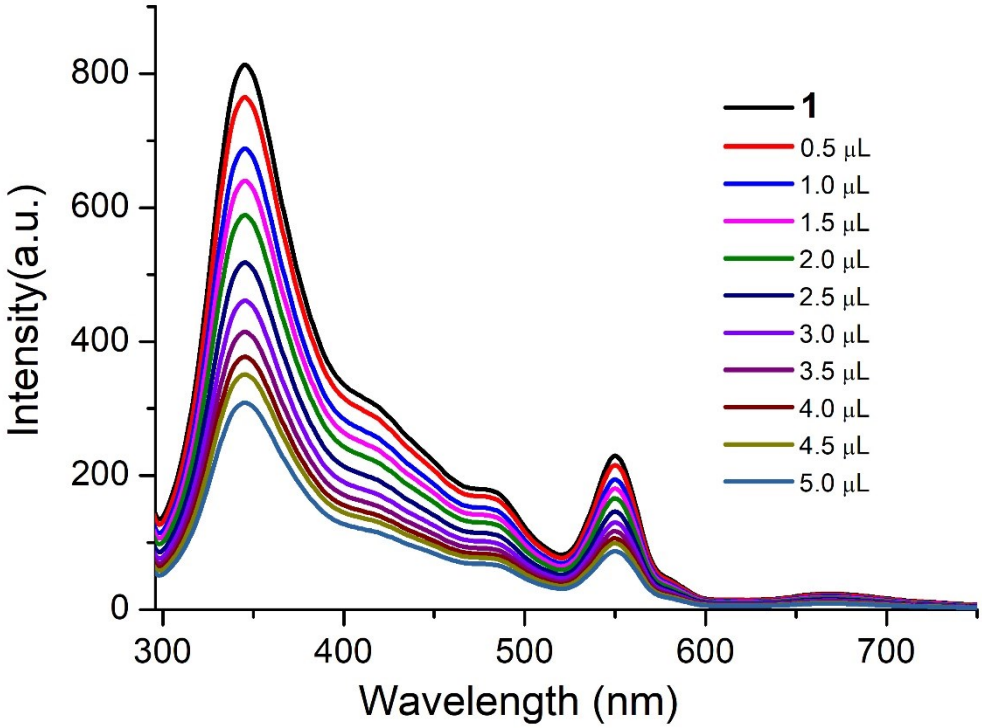

Fig. S5: The change in fluorescence intensity of **1** upon incremental addition of 2,4-DNP solution in Water.

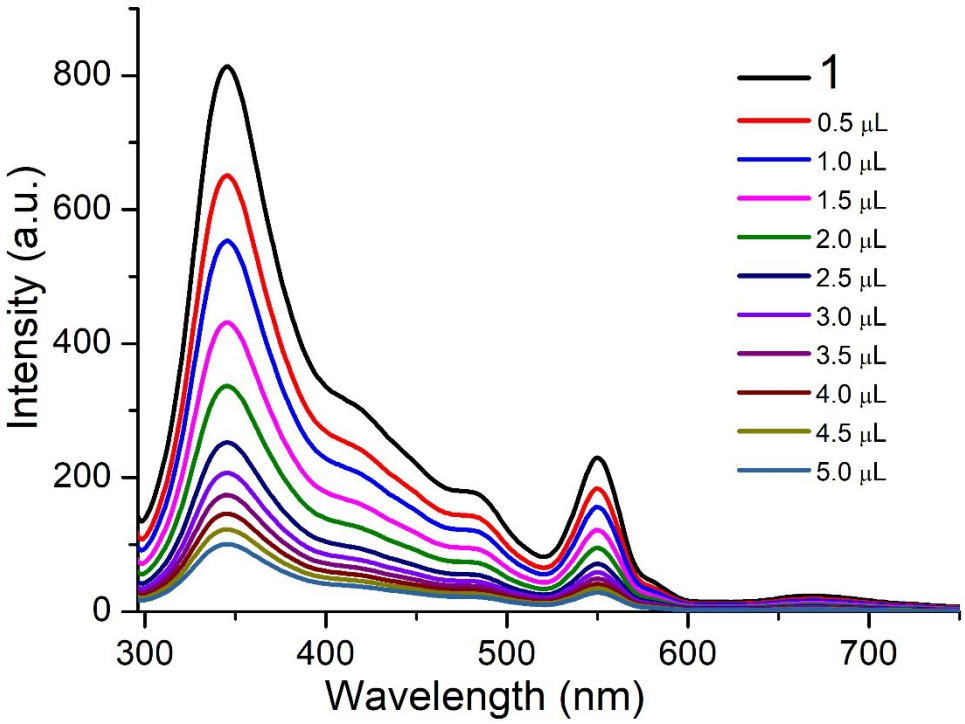

Fig. S6: The change in fluorescence intensity of **1** upon incremental addition of PA solution in Water.

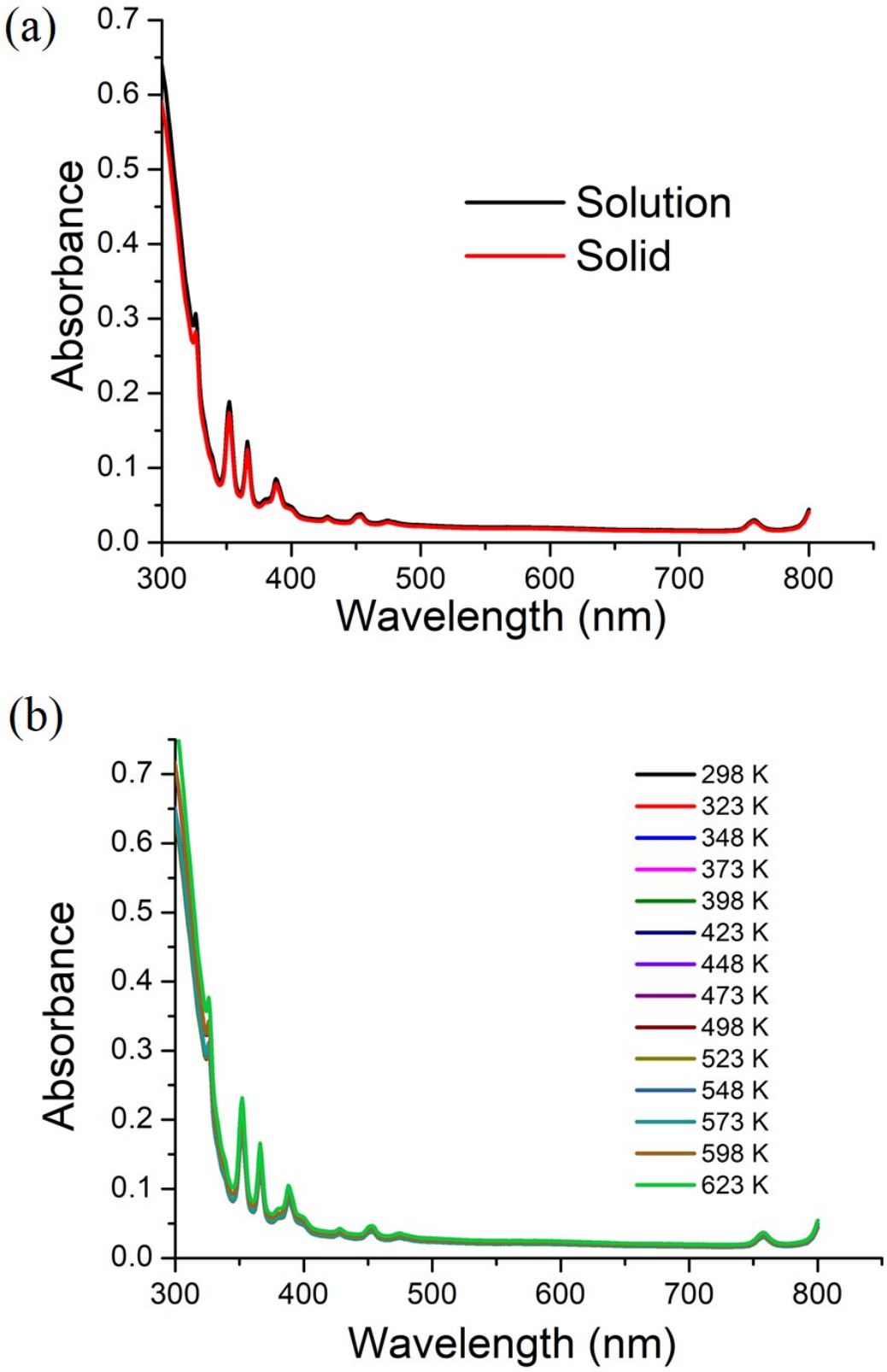

Fig. S7: (a) Solid and solution (water) state UV-Visible spectra of **1.** (b) UV-Visible spectra at different temperature.

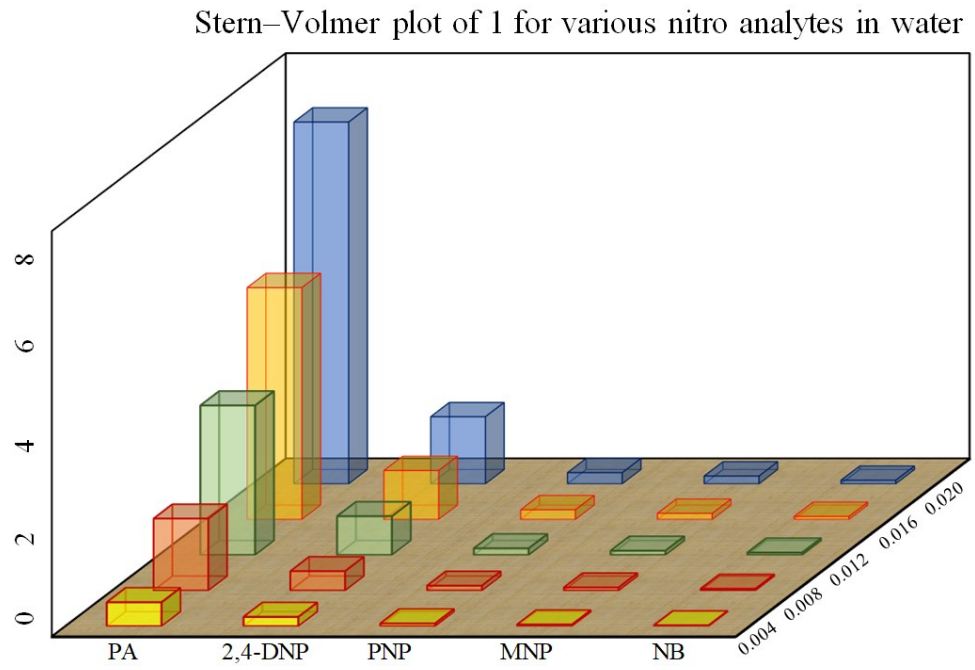

Fig. S8: 3D representation of Stern-Volmer (SV) plots of **1** for various NACs.

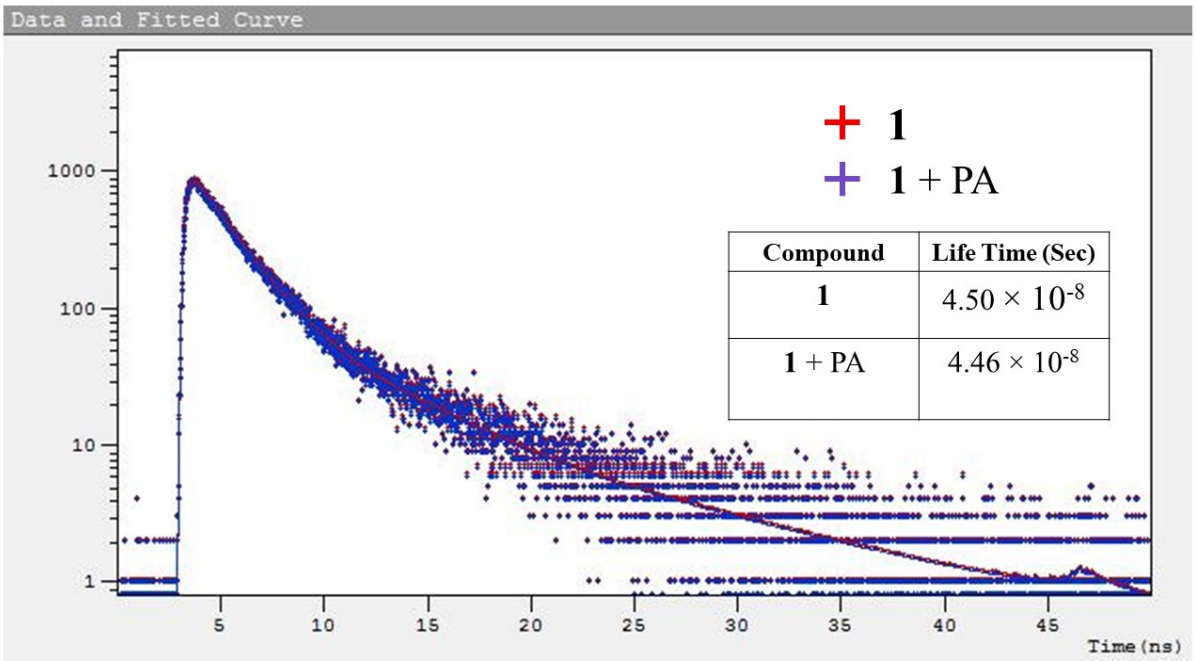

Fig. S9: Fluorescence decay profile of **1** in the presence and absence of PA solution.

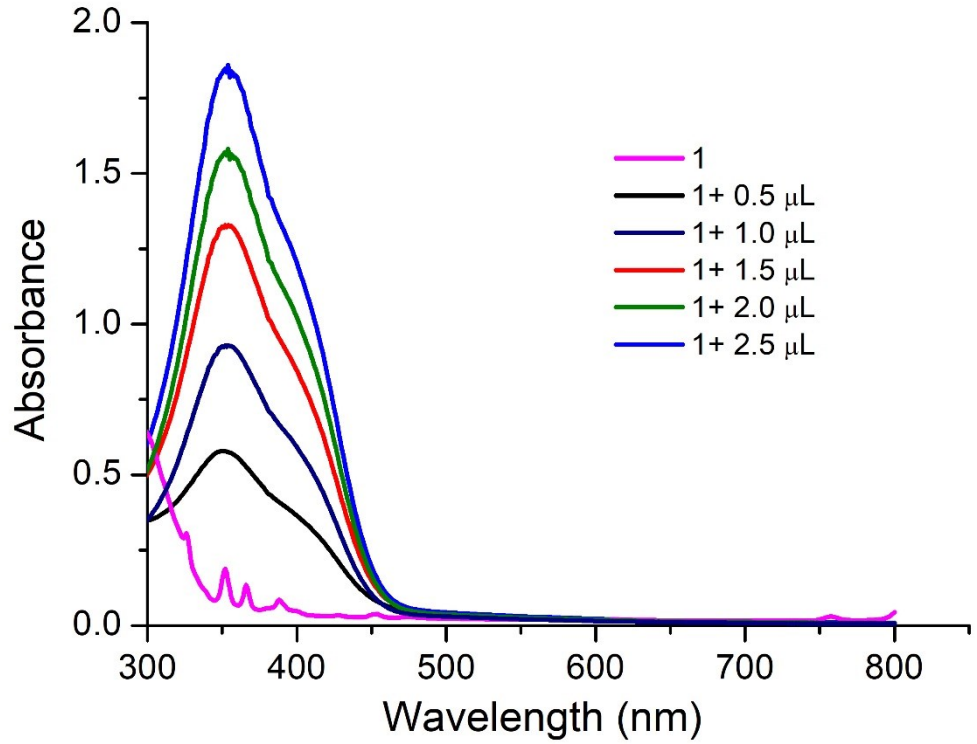

Fig. S10: UV-vis spectra of **1** upon gradual addition of PA showing spectral change with the appearance of new band at 352 nm.

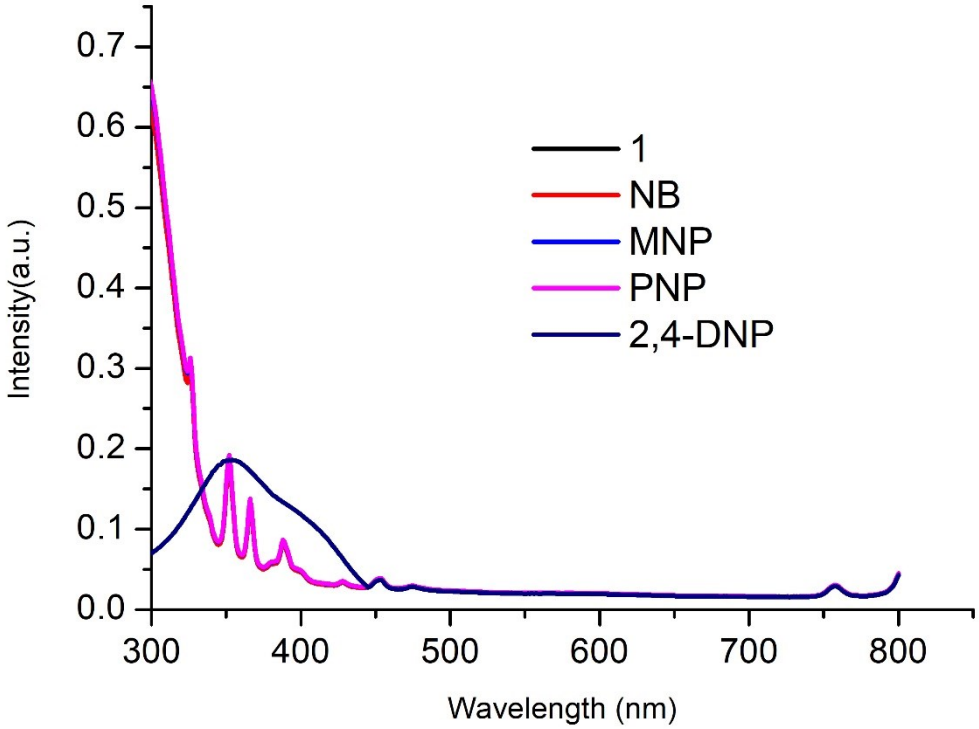

Fig. S11: UV-vis spectra of **1** in the presence of different nitro analytes.

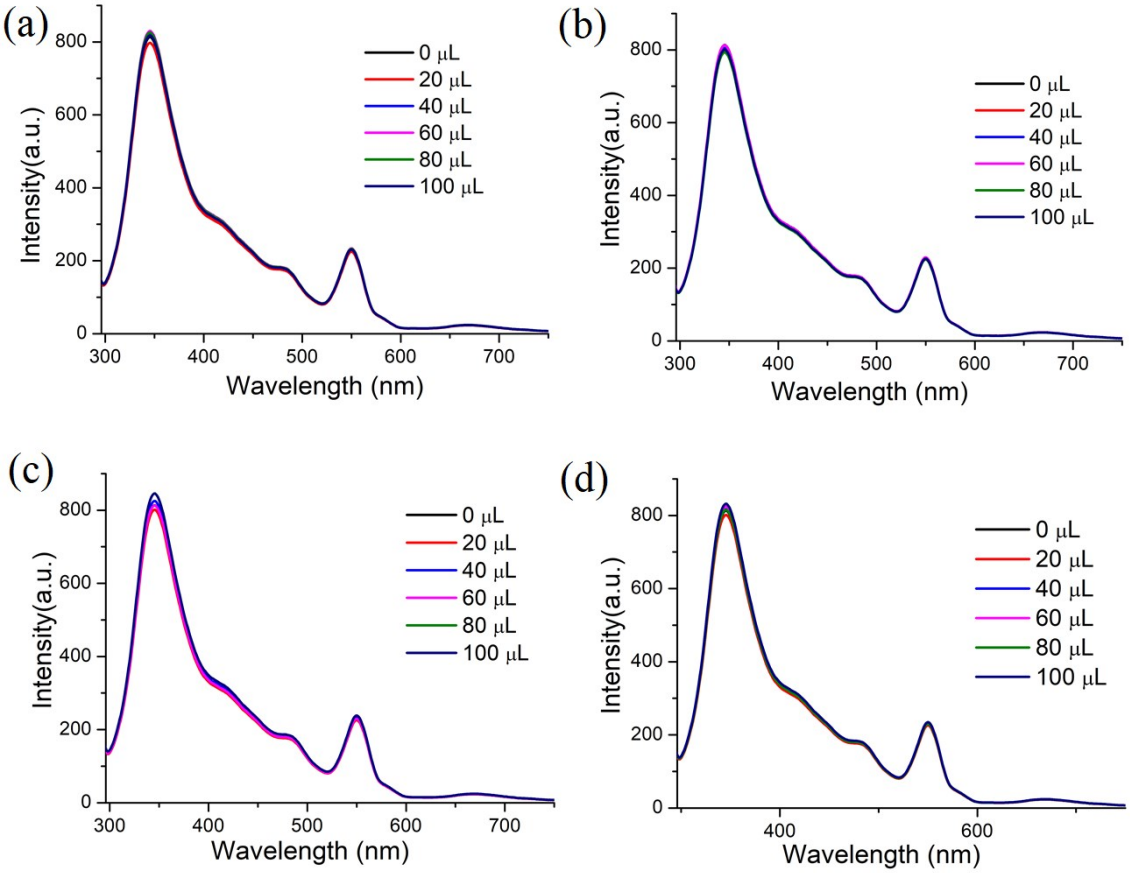

Fig. S12: The change in fluorescence intensity of **1** upon incremental addition of Catechol (**a**), 2,6 Bis(hydroxymethyl) p-cresol (**b**), di(trimethylolpropane) (**c**) and 1,1,1-Tris(hydroxymethyl)propane (**d**) (1mM) solution in Water.

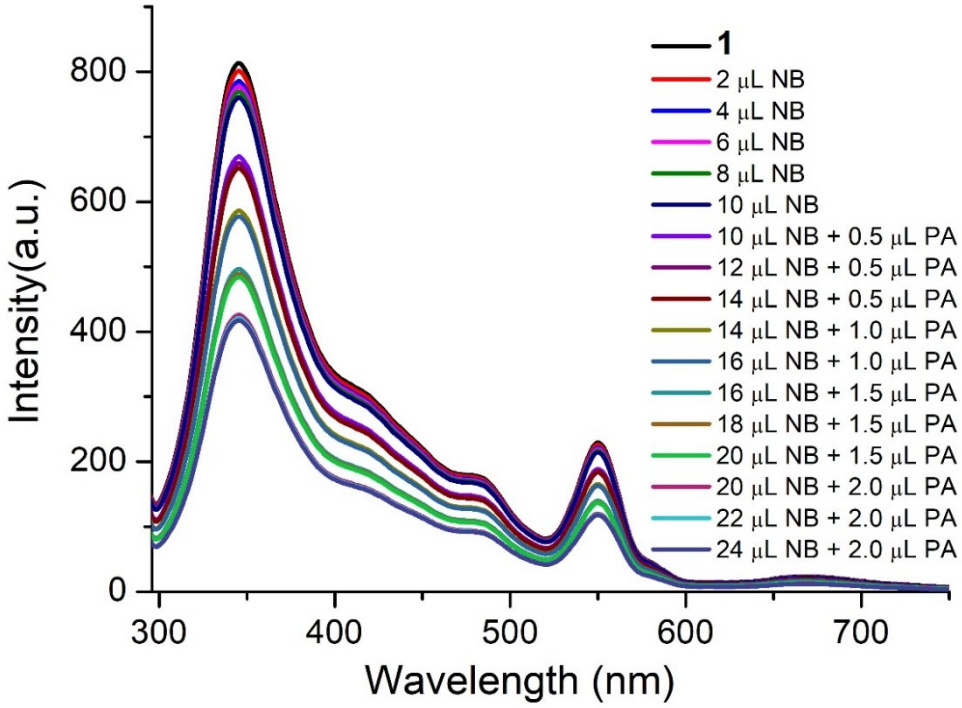

Fig. S13: The change in fluorescence intensity of **1** upon addition of NB followed by PA.

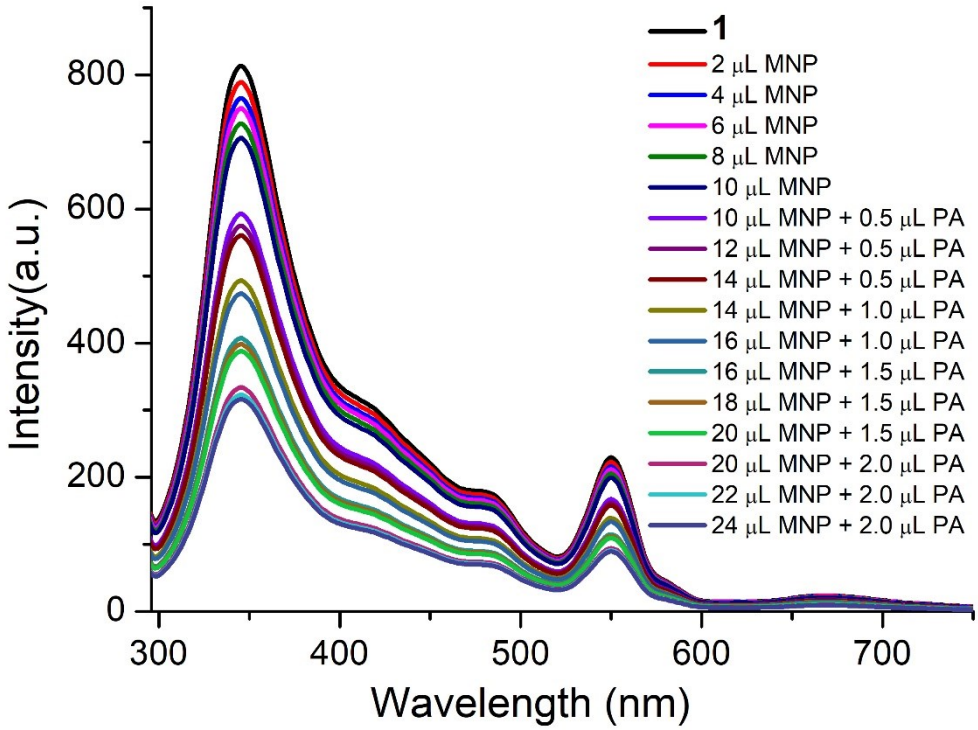

Fig. S14: The change in fluorescence intensity of **1** upon addition of MNP followed by PA.

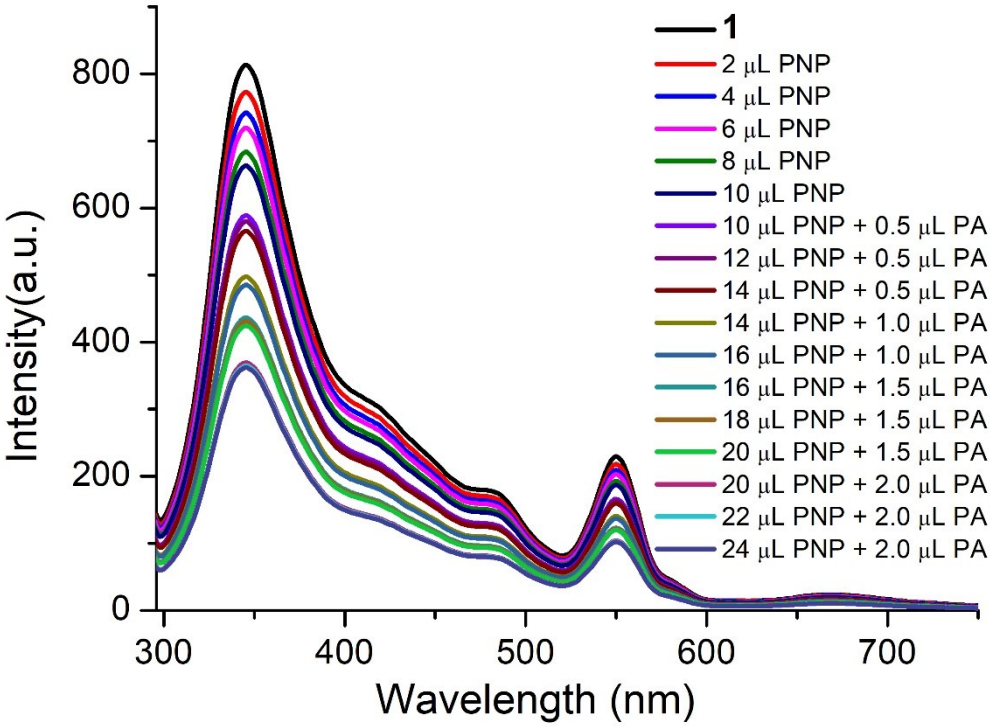

Fig. S15: The change in fluorescence intensity of **1** upon addition of PNP followed by PA.

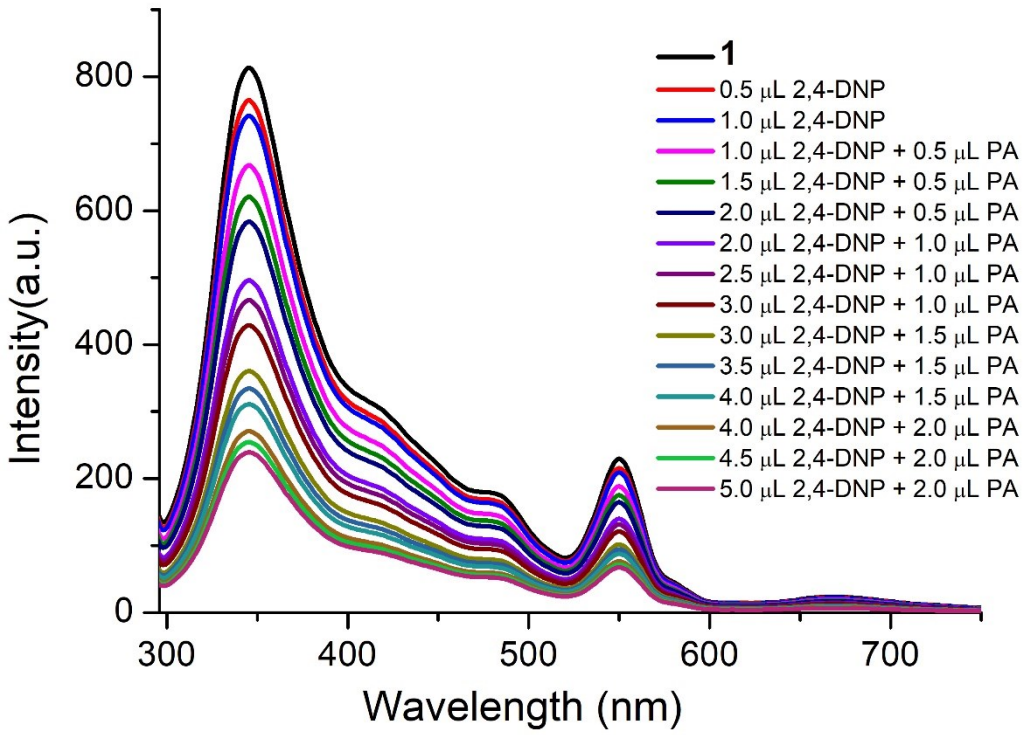

Fig. S16: The change in fluorescence intensity of **1** upon addition of 2,4-DNP followed by PA.

Table S2: - HOMO and LUMO energies calculated for nitroanalytes at B3LYP/6- 31G* level of theory.

Analytes	HOMO (ev)	LUMO (eV)	Band gap (eV)
NB	-7.752	-3.023	4.729
PNP	-7.236	-2.722	4.514
MNP	-7.029	-2.984	4.045
2,4-DNP	-6.408	-3.014	3.394
PA	-8.205	-4.384	3.821

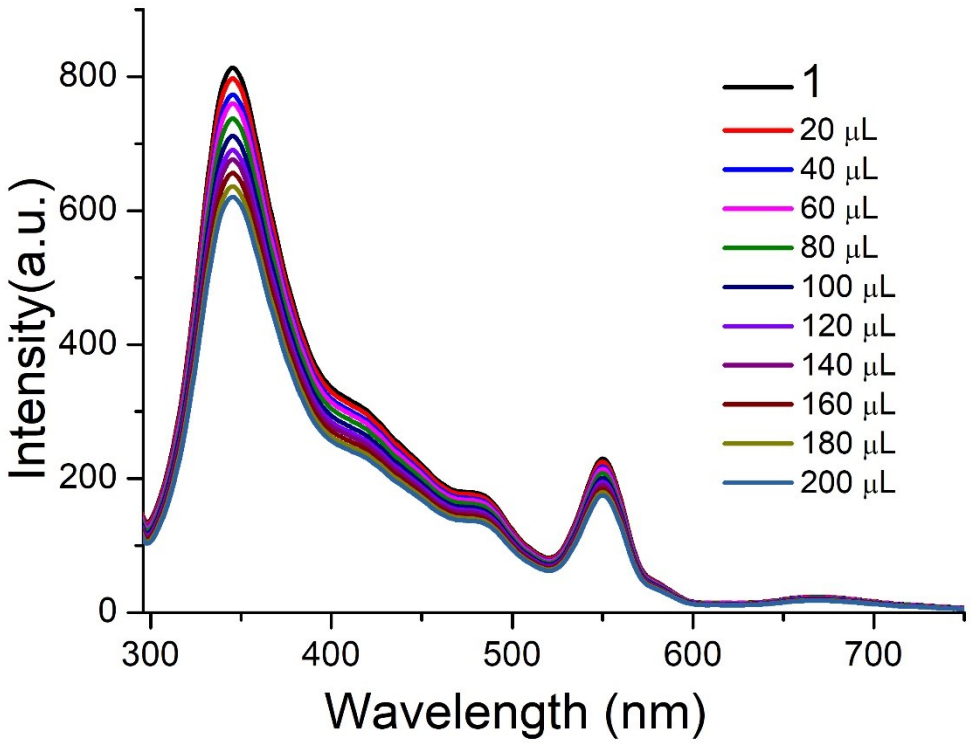

Fig. S17: Emission spectrum of **1** upon incremental addition of Cd^{2+} (1mM) solution in Water.

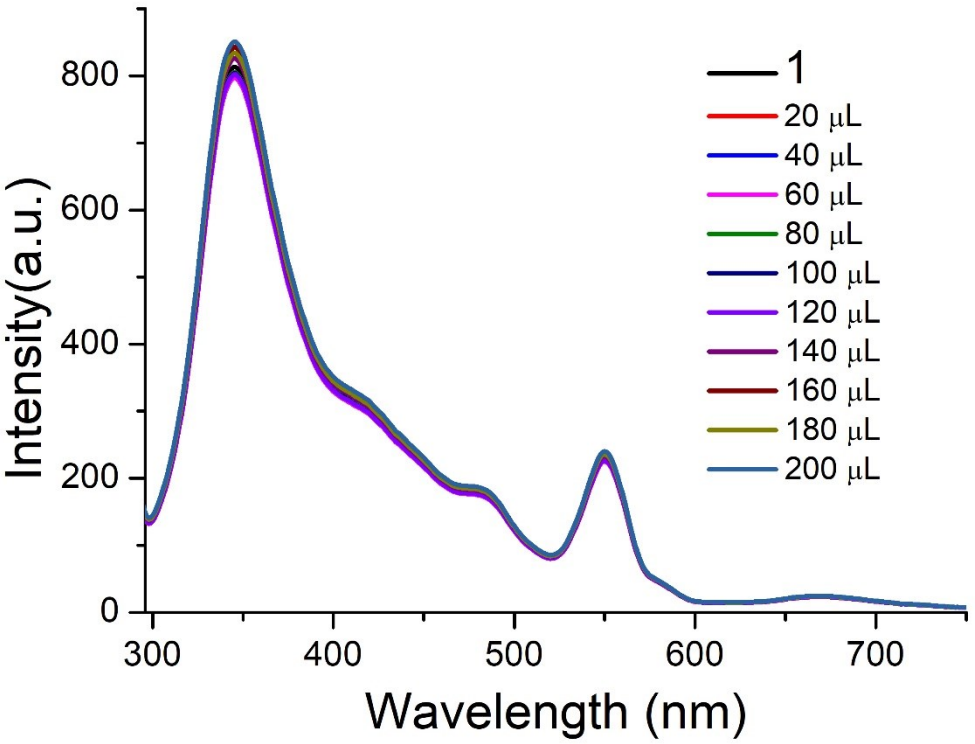

Fig. S18: Emission spectrum of **1** upon incremental addition of Co^{2+} (1mM) solution in Water.

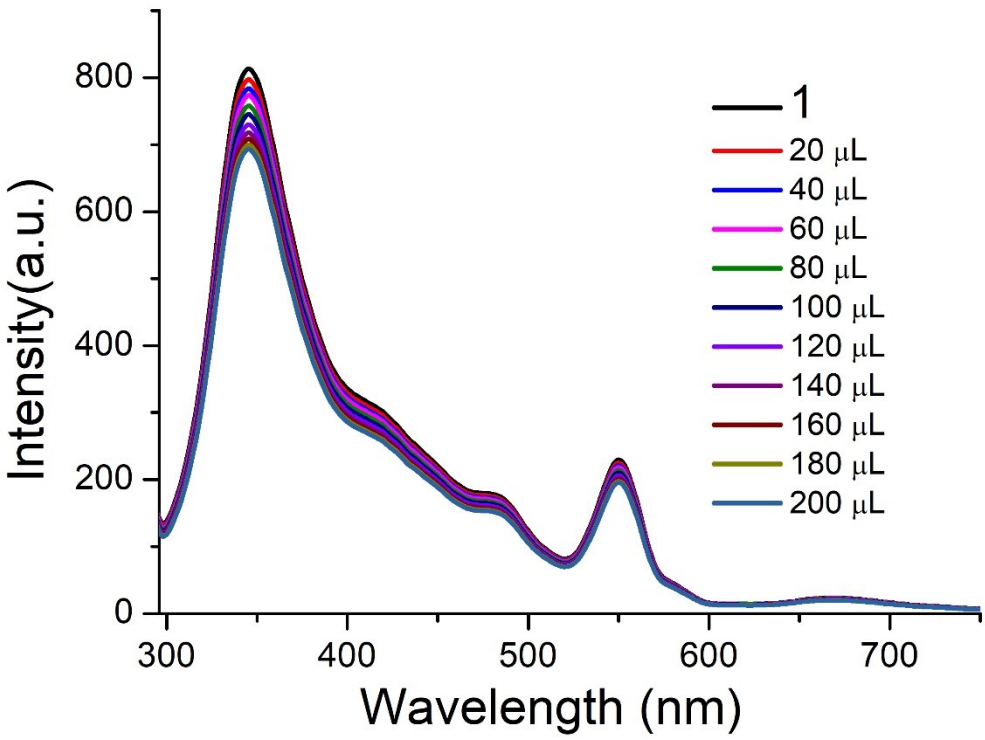

Fig. S19: Emission spectrum of **1** upon incremental addition of Cr^{3+} (1mM) solution in Water.

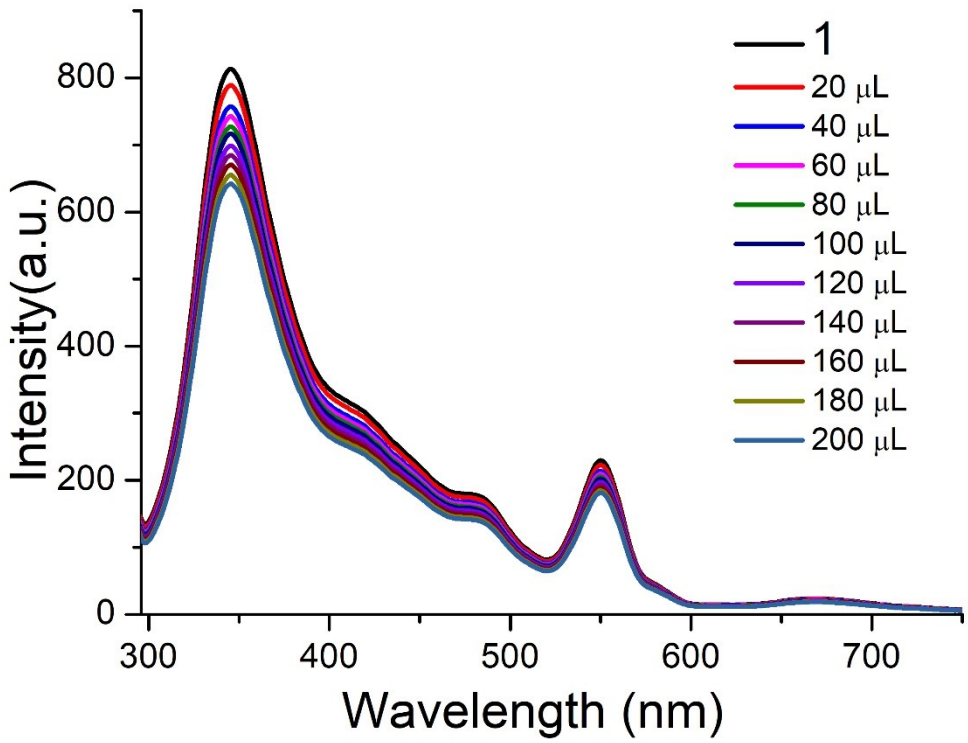

Fig. S20: Emission spectrum of **1** upon incremental addition of Cu^{2+} (1mM) solution in Water.

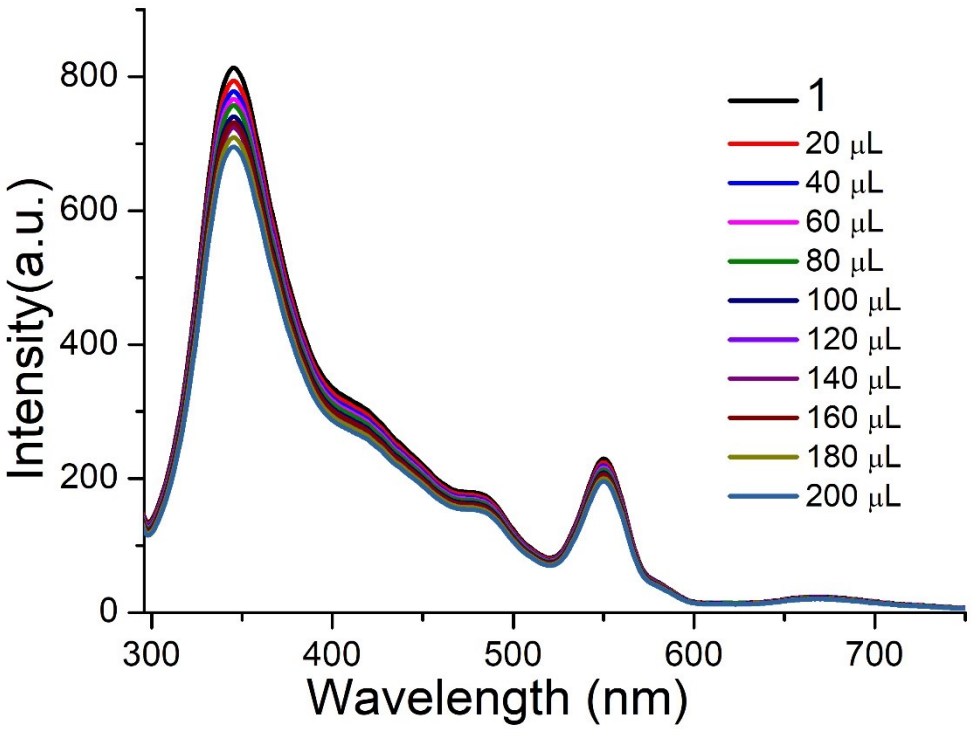

Fig. S21: Emission spectrum of **1** upon incremental addition of Hg^{2+} (1mM) solution in Water.

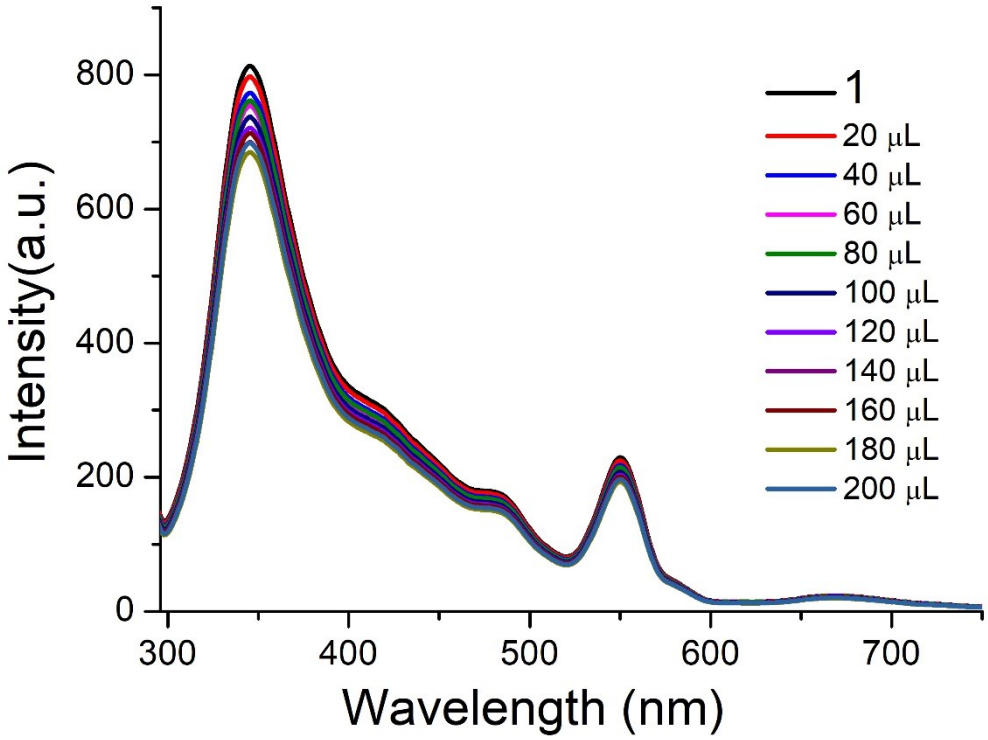

Fig. S22: Emission spectrum of **1** upon incremental addition of Ni^{2+} (1mM) solution in Water.

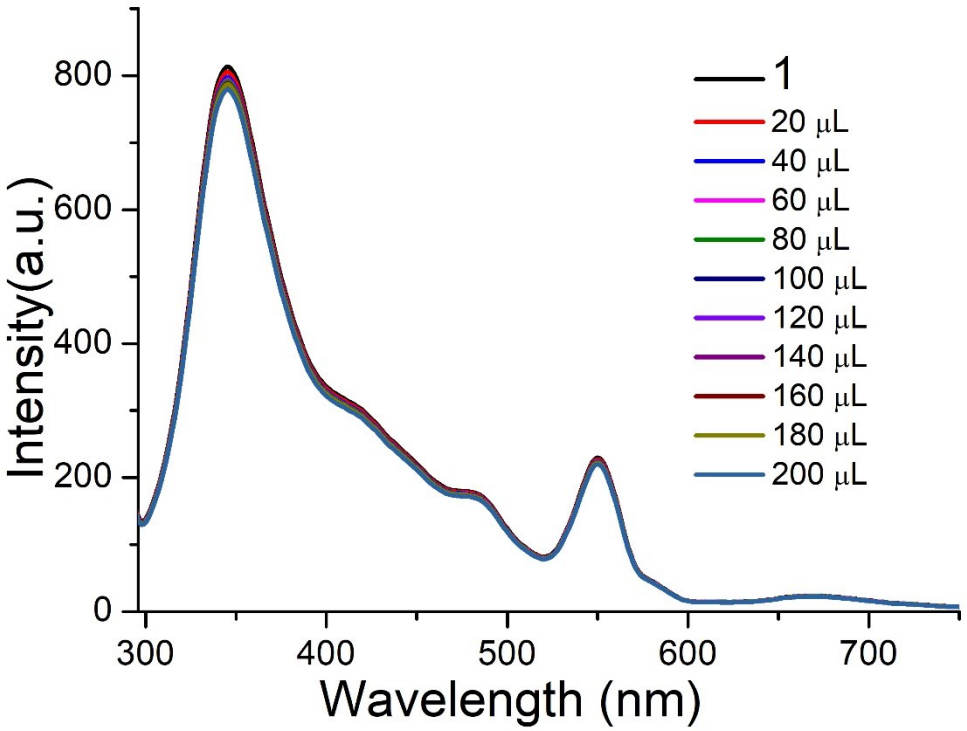

Fig. S23: Emission spectrum of **1** upon incremental addition of Pb^{2+} (1mM) solution in Water.

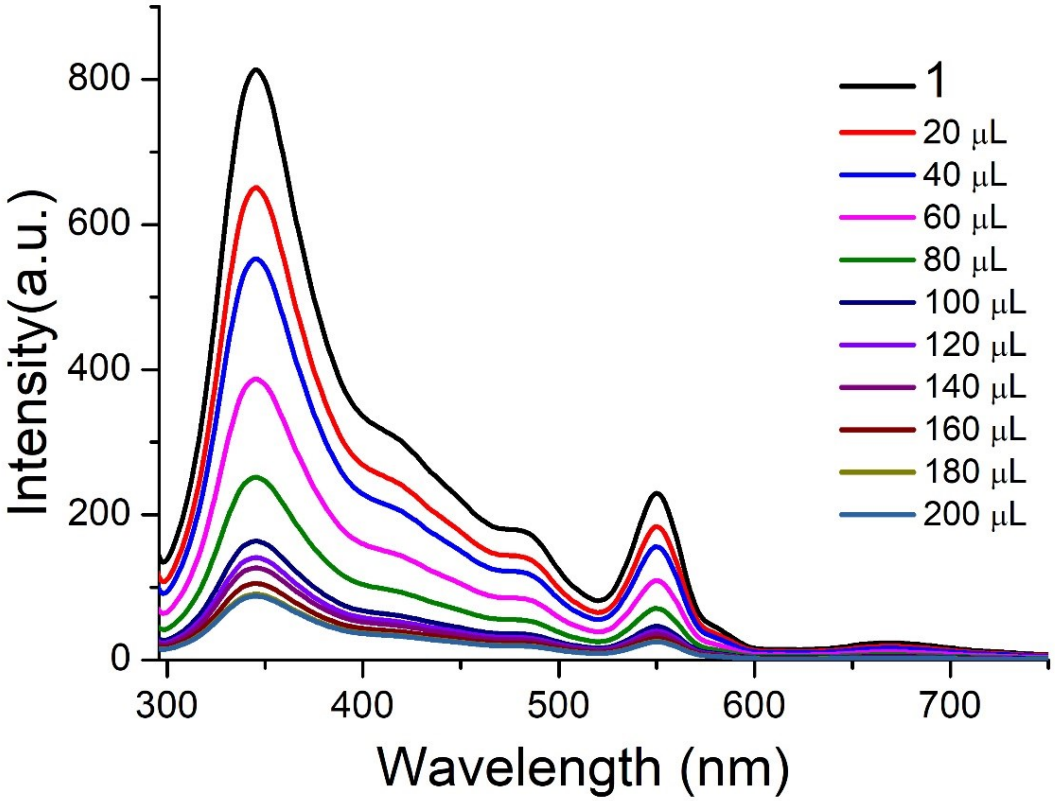

Fig. S24: Emission spectrum of **1** upon incremental addition of Fe^{3+} (1mM) solution in Water.

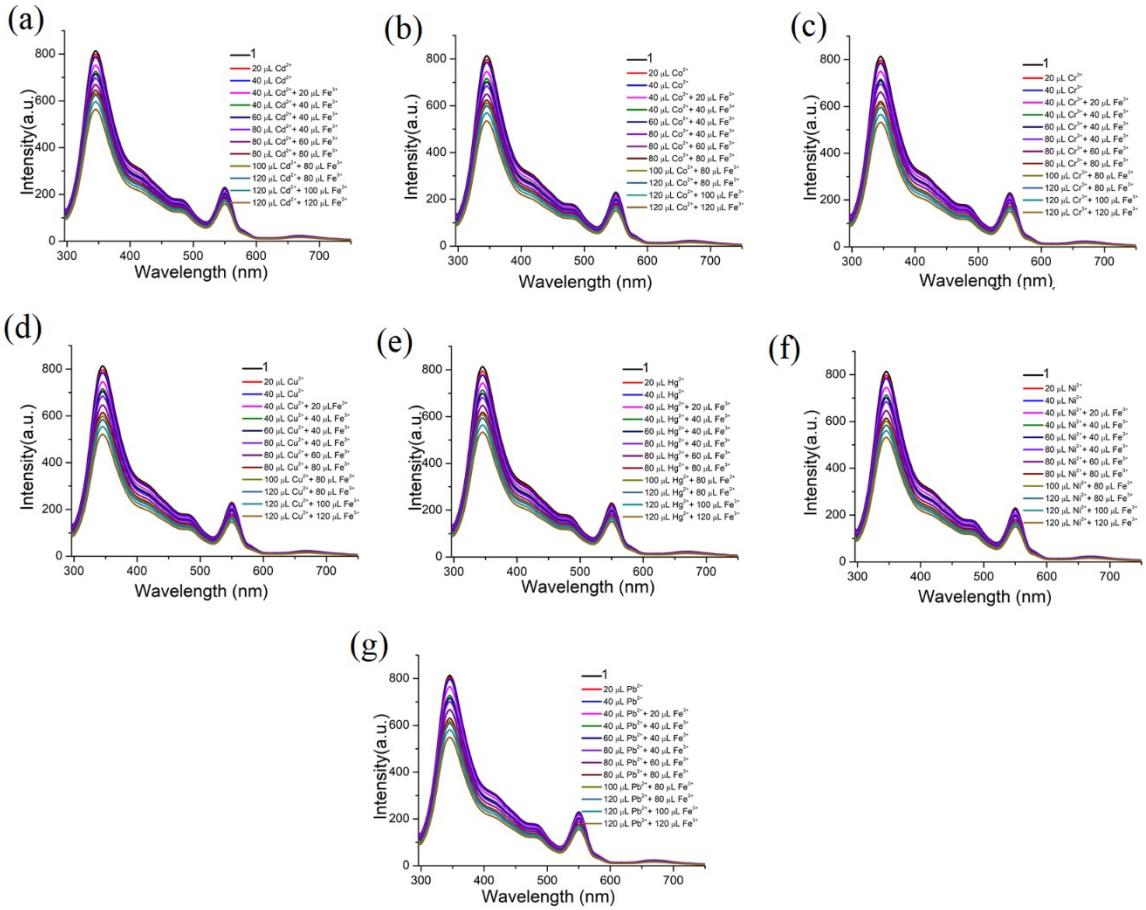

Fig. S25: The change in fluorescence intensity of **1** upon addition of Cd^{2+}(a), Co^{2+}(b), Cr^{3+}(c) Cu^{2+}(d), Hg^{2+}(e), Ni^{2+}(f) and Pb^{2+}(g) solution followed by Fe^{3+} solution respectively.

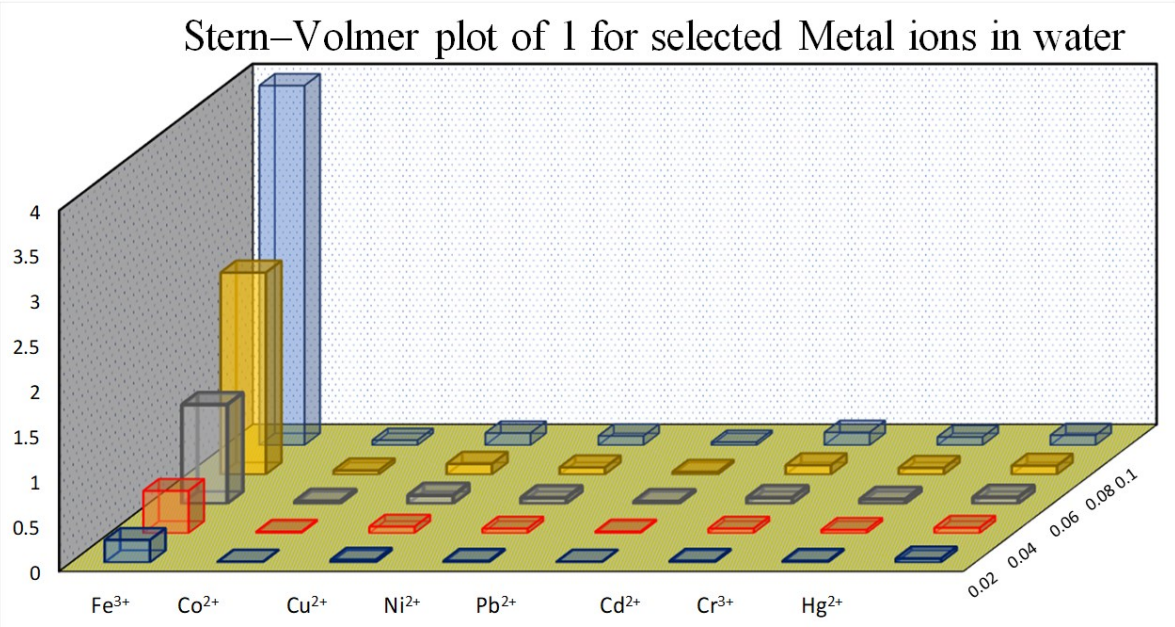

Fig. S26: 3D representation of Stern-Volmer (SV) plots of **1** for different metal ions.

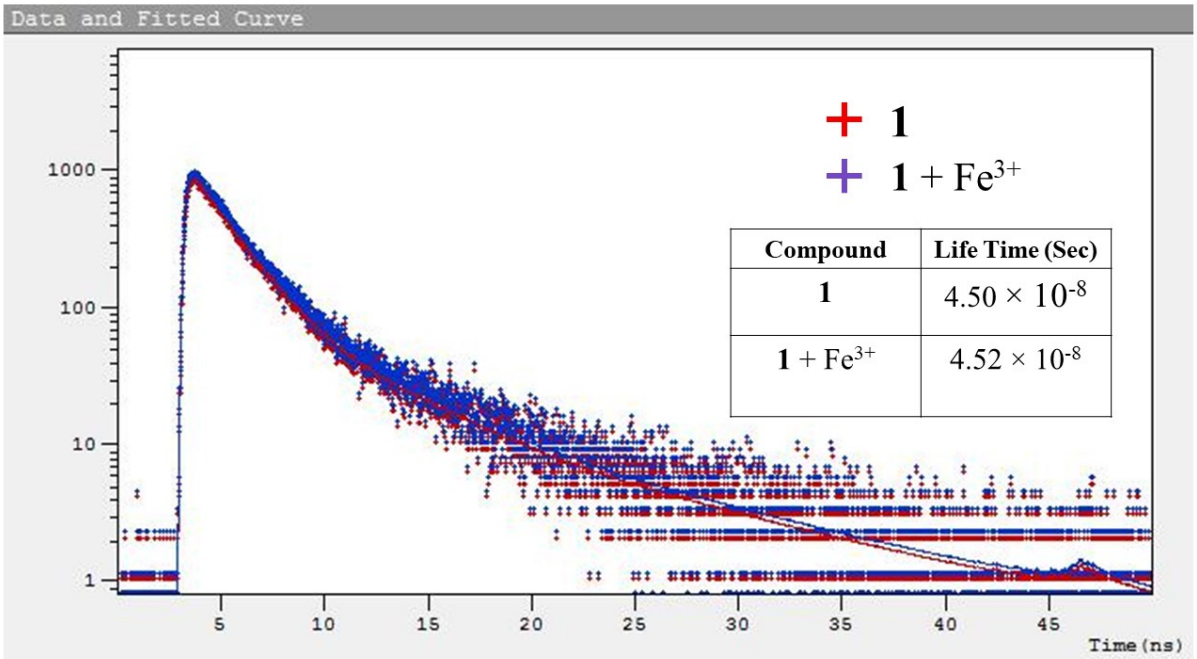

Fig. S27: Fluorescence decay profile of **1** in the presence and absence of Fe^{3+} ions.

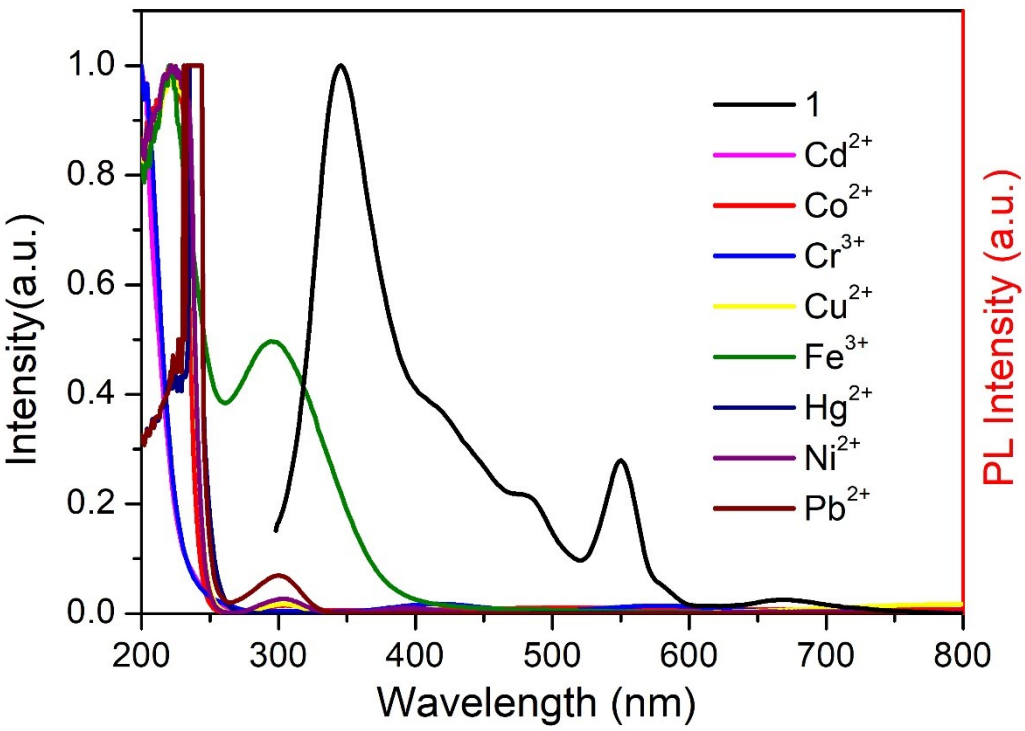

Fig. S28: Spectral overlap between normalized emission spectra of **1** (λ_{ex} = 296 nm) and normalized absorbance spectra of the selected metal ions.

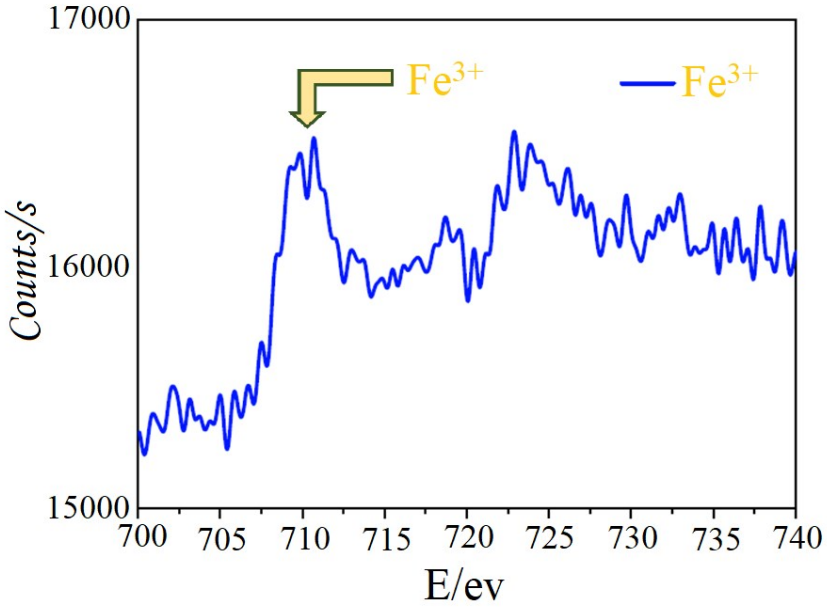

Fig. S29: XPS of Fe^{3+} shows the typical peak of Fe^{3+} at 710 eV.

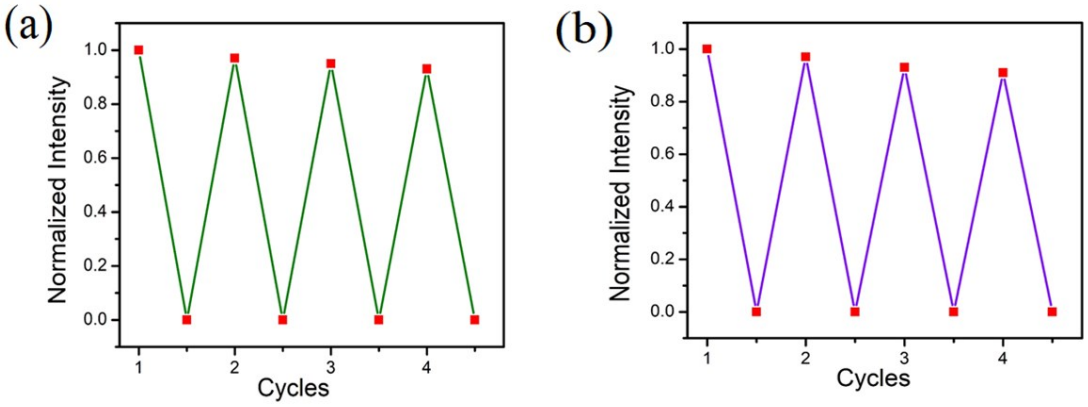

Fig. S30: The quenching and recyclability test of **1**, the upper dots represent the initial luminescence intensity and the lower dots represent the intensity upon addition of (a) 5.49ppb of PA, (b) 27.9 ppb of Fe^{3+} solution.

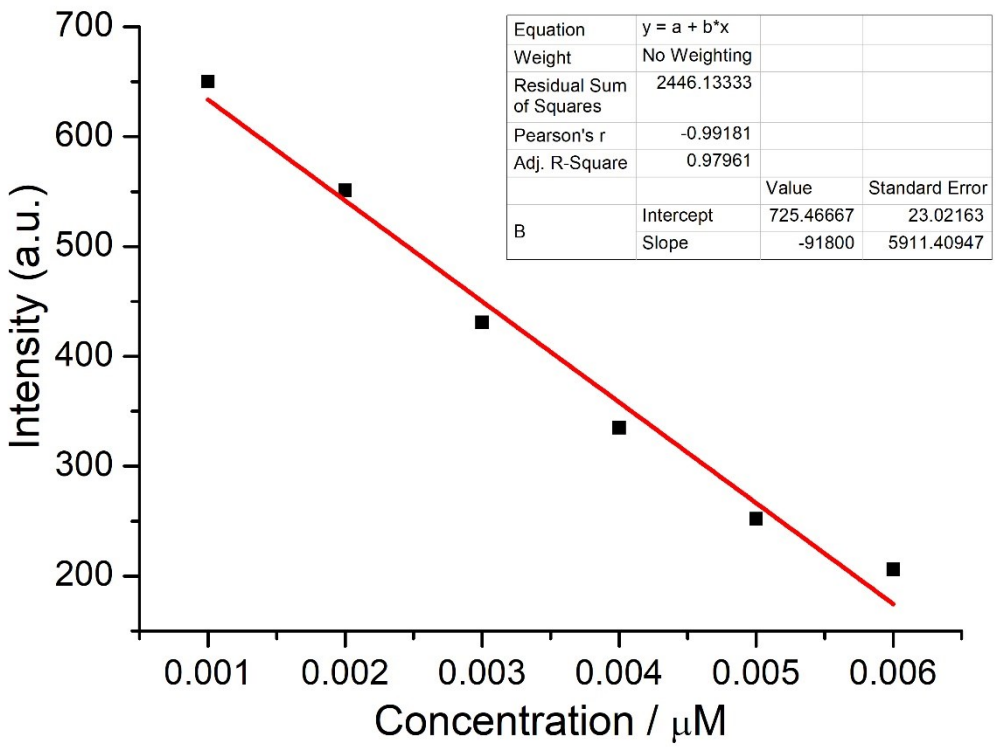

Fig. S31: Linear region of fluorescence intensity of **1** in water upon addition of PA (0.5 – 3 μL, 2 mM stock solution) in water.

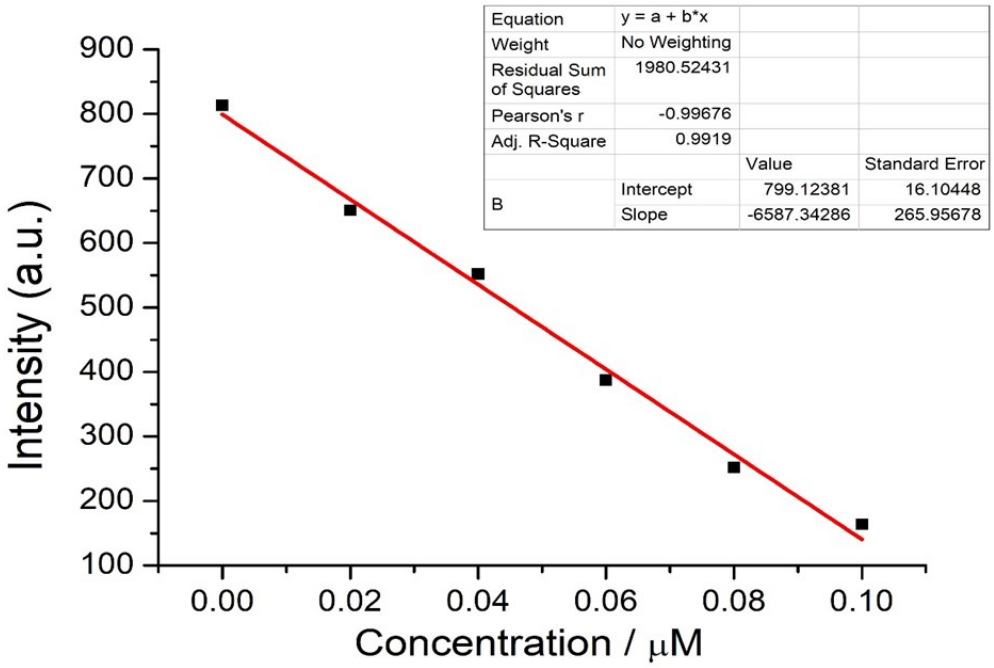

Fig. S32: Linear region of fluorescence intensity of **1** in water upon addition of Fe^{3+} (20 – 100 μL, 1 mM stock solution) in water.

Table S3. Selected bond lengths and angles for **1**.

Bond Length (**1**)			
Dy1–O2	2.332(7)	Dy3–O2	2.340(7)
Dy1–O3	2.337(8)	Dy3–O5	2.340(8)
Dy1–O4	2.344(7)	Dy3–O3	2.346(7)
Dy1–O5	2.346(8)	Dy3–O5W	2.431(9)
Dy1–O2W	2.443(11)	Dy3–O6W	2.466(9)
Dy1–O1	2.5062(5)	Dy3–O1	2.5034(5)
Dy1–O6	2.508(9)	Dy3–O13	2.517(9)
Dy1–O1W	2.512(11)	Dy3–O12	2.568(9)
Dy1–O7	2.538(9)	N1–O6	1.218(15)
Dy1–N1	2.934(10)	N1–O8	1.245(14)
Dy2–O5	2.343(7)	N1–O7	1.251(15)
Dy2–O2	2.353(8)	N2–O11	1.220(12)
Dy2–O4	2.362(8)	N2–O9	1.245(12)
Dy2–O3	2.372(7)	N2–O10	1.279(12)
Dy2–O3W	2.436(11)	N3–O14	1.233(12)
Dy2–O4W	2.443(8)	N3–O13	1.238(13)
Dy2–O1	2.4799(5)	N3–O12	1.279(13)
Dy2–O10	2.503(8)	N4–O16	1.09(2)
Dy2–O9	2.590(8)	N4–O15	1.27(3)
Dy3–O4	2.334(7)	N4–O17	1.306(18)
Bond angles (**1**)			
O2–Dy1–O3	79.5(3)	O3–Dy1–O6	80.6(3)
O2–Dy1–O4	129.9(3)	O4–Dy1–O6	73.1(3)
O3–Dy1–O4	80.3(3)	O5–Dy1–O6	133.4(3)
O2–Dy1–O5	80.6(3)	O2W–Dy1–O6	102.1(4)
O3–Dy1–O5	129.5(3)	O1–Dy1–O6	128.5(3)
O4–Dy1–O5	78.1(3)	O2–Dy1–O1W	78.9(3)
O2–Dy1–O2W	76.9(3)	O3–Dy1–O1W	73.4(4)
O3–Dy1–O2W	140.4(3)	O4–Dy1–O1W	136.2(4)
O4–Dy1–O2W	138.8(3)	O5–Dy1–O1W	145.2(4)
O5–Dy1–O2W	76.9(3)	O2W–Dy1–O1W	71.2(4)
O2–Dy1–O1	65.44(19)	O1–Dy1–O1W	128.7(3)
O3–Dy1–O1	65.09(17)	O6–Dy1–O1W	68.6(4)
O4–Dy1–O1	64.50(18)	O2–Dy1–O7	146.2(3)
O5–Dy1–O1	64.38(18)	O3–Dy1–O7	129.4(3)
O2W–Dy1–O1	128.9(3)	O4–Dy1–O7	78.2(3)
O2–Dy1–O6	145.5(3)	O5–Dy1–O7	89.5(3)
O2W–Dy1–O7	69.4(3)	O2–Dy1–N1	155.4(3)
O1–Dy1–O7	137.5(3)	O3–Dy1–N1	104.7(3)
O6–Dy1–O7	49.4(3)	O4–Dy1–N1	74.4(3)
O1W–Dy1–O7	92.1(4)	O5–Dy1–N1	112.4(3)

Calculation of standard deviation:

Table S4: Standard deviation for **1**.

Blank Readings (only probe)	FL Intensity of **1**
Reading 1	813.44
Reading 2	821.57
Reading 3	817.23
Reading 4	821.95
Reading 5	814.87
Standard Deviation (σ)	**3.44**

Calculation of Detection Limit:

Table S5: Detection limit calculation of **1** for PA

Complex	Slope from Graph (m)	Detection limit ($3\sigma/m$)	
		μM	ppb
1	91800	1.12E-04	~0.03

Table S6: Detection limit calculation of **1** for Fe^{3+}

Complex	Slope from Graph (m)	Detection limit ($3\sigma/m$)	
		μM	ppb
1	6587.34	1.57E-03	~0. 09

Table S7: Summary of Shape analysis of **1**

EP-9	**1**	D9h	Enneagon
OPY-9	**2**	C8v	Octagonal pyramid
HBPY-9	**3**	D7h	Heptagonal bipyramid
JTC-9	**4**	C3v	Johnson triangular cupola J3
JCCU-9	**5**	C4v	Capped cube J8
CCU-9	**6**	C4v	Spherical-relaxed capped cube
JCSAPR-9	**7**	C4v	Capped square antiprism J10
CSAPR-9	**8**	C4v	Spherical capped square antiprism
JTCTPR-9	**9**	D3h	Tricapped trigonal prism J51

TCTPR-9	**10**	D3h	Spherical tricapped trigonal prism
JTDIC-9	**11**	C3v	Tridiminished icosahedron J63

Complex	**[ML_9]**	EP-9	OPY-9	HBPY-9	JTC-9	JCCU-9	CCU-9	JCSAPR-9	**CSAPR-9**	JTCTPR-9	TCTPR-9	JTDIC-9
1		34.005	21.601	18.952	14.419	9.789	9.422	1.537	**1.097**	2.762	2.099	14.487

Quantum Yields: Fluorescence quantum yields from fluorescence emission spectra of the complexes in water were calculated with quinine sulphate (φ = 0.54) and Refractive Index: water = 1.33 as standard by using following equation:

$$\frac{\varphi Complex}{\varphi Q.S.} = \frac{Area\ of\ the\ complex}{Area\ of\ Q.S.} X \frac{Absorbance\ of\ Q.S.}{Absorbance\ of\ Complex} X \frac{(R.I.\ of\ solvent)^2}{(R.I.\ of\ Water)^2}$$

Φ = Quantum Yield; R.I. = Refractive Index, Q.S. = Quinoline sulphate